Remote Research Experience at Oregon State University

# PPTA and NanoGrav 15- Worth to compare for Individual Pulsars?

Jyotsna Patil

## Abstract

Comparing all the sensitivity curves in IPTA made it curious whether individual pulsars possess the same properties as the sensitivity curves of combined data sets, such as a bump in the sensitivity curve due to not counting DM variations due to the solar wind. That led to comparing the sensitivity curves of individual pulsars and finding solar wind electron density diagrams for the pulsars using NE_SW values.

**Keywords**
PPTA, NanoGrav, Sensitivity curves, Solar Wind

## 1 Introduction

The International PTA published results of a comparison of various PTA collaborations that are present worldwide. One such comparison includes a comparison of sensitivity curves of EPTA+InPTA, PPTA, and NanoGrav. Sensitivity curves are constructed using different timing and noise modeling techniques. PPTA also included DM variations due to solar wind while constructing the sensitivity curve, but it was left out when compared with PPTA and EPTA+ InPTA. That left a small bump at 2.76 nHz in the diagram. That led to finding the bump due to not counting solar wind in individual pulsars in two datasets- viz.PPTA and NanoGrav.To achieve this goal, we selected identical pulsars from both datasets. They are J1713+0747, J2124-3358, and J2145-0750.

Well, though while starting, it was all about finding bumps in the sensitivity curves, later on, due to the complexity of the problem, the problem was divided into two sections-

1)Comparing sensitivity curves of individual pulsars from two datasets by using TOAs

2)To find delay due to DM of solar wind in the same pulsars by considering NE_SW values and constructing solar wind electron density diagrams for the same pulsars.

However, sensitivity curves were constructed using both timing and noise modeling. Here, a comparison is quite incomplete because of the use of only TOAs. Also,for NAnoGrav datasets, solar wind delay and solar diagrams, solar wind is absorbed in DMX values. Thus, solar wind delay and solar wind electron density diagrams become less significant for NanoGrav datasets.

## 2 Methods

Before starting the data analysis, the NG 15 years and PPTA 3rd data releases were obtained from their respective websites. The same pulsars were chosen from both data sets on the basis of careful observations. Those are J1713+0747, J2124-3358, and J2145-0750 respectively.

The data files used here are .tim files. The .tim files contain information related to TOAs, such as TOA in MJD, TOA error, and frequency of the receiver telescope. They also document a variety of information related to the telescope. However, our interest is only in the TOA and TOA error columns.

The software used to construct the sensitivity curves is Hasasia. It is available in the Python library and API in the GitHub repository. The simplest way to construct sensitivity curves is by using the hasasia.Sensitivity.Pulsar and hasasia.sensitivity.Spectrum class. The inputs for this class consist of times of arrival (TOAs) in seconds. Before data analysis, we extracted the TOAs and the TOA error columns from the.tim files. Since the TOAs are recorded in Modified Julian Date (MJD) format, they are converted into seconds. We utilized the Time class from the Astropy library for this conversion. Additionally, the coordinates of the pulsar's location in the sky are provided in degrees, minutes, and seconds format, which was converted into radians. The sensitivity curves were constructed in Hasasia using the above data.

The SolarWindDispersion() class in the PINT software is designed to calculate delays

caused by the solar wind, measured in seconds. The class requires a parameter known as TOAs. This information is also relevant in this context. It is important to note that the class depends on the NE_SW value. In the parameter files for both PPTA and NG15, the NE_SW value is set to 0. As a result, the delay for every pulsar in this situation is also 0. Since solar wind delay values are typically non-zero,the NE_SW value from the noise files is used instead.

By analyzing the NE_SW values from the noise files, we can construct diagrams of solar wind delay and solar wind behavior. In the case of NG15, the solar wind is integrated into the DMX value, while the NE_SW values are only in the PPTA data files. The respective NE_SW values are as follows:

J1713+0747 = 5.0206514446838589999

J2124-3358 = 5.744822249890441

J2145-0750 = 6.0118246308458179999

The formula used to calculate solar wind delay is as follows.

$$\Delta t = \frac{e^2}{2\pi m_e c^2} \frac{DM}{v^2} \tag{1}$$

Thus, by putting values of e, $m_e$ , and c, the formula becomes,

$$\Delta t = 4.15 \times 10^3 \frac{DM}{v^2} \tag{2}$$

Where $v$ represents the frequency of the radio frequency. And $\Delta t$ is delayed due to DM.

Also, we know that

$$DM = \int_0^d n_e \, dl \tag{3}$$

Thus, for convenience, the new values are considered as NE_SW. In the formula, replace the DM value with the NE_SW value. So, the formula becomes

$$\Delta t = 4.15 \times 10^3 \frac{NE\_SW}{v^2} \tag{4}$$

The delays caused by solar wind and the solar wind electron density for each pulsar are calculated for datasets using the previously mentioned formula. The radio frequency mentioned here is obtained from the .tim files for each pulsar.

# 3 Results

In the beginning, the first set of results shows the sensitivity curve of the pulsars. The figures are as follows:

The following figure represents a comparison of the sensitivity curves of the pulsars.

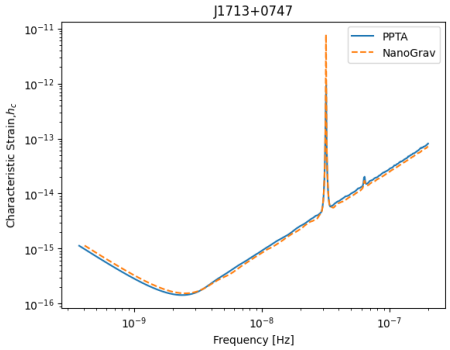


Figure 1: Sensitivity Curves of J1713+0747

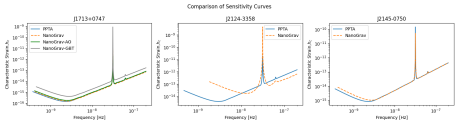

Figure 2: Comparison of Sensitivity Curves

The above figure 2 represents the sensitivity curves for different pulsars from both datasets. The first figure represents the sensitivity curves for pulsar J1713+0747, the most sensitive pulsar. Separate observations were made using the Parkes, Arecibo, and Green Bank telescopes. The datasets collected from these telescopes are available and their respective sensitivity curves, shown in the figure, exhibit insignificant differences.

The pulsars J2124-3358 and J2145-0750 each have two curves in their respective figures, representing two different datasets. For J2124-3358, the short observation period of the NanoGrav dataset results in a significant difference in the sensitivity curves. This suggests that the duration of the observations is a crucial factor in constructing sensitivity curves.

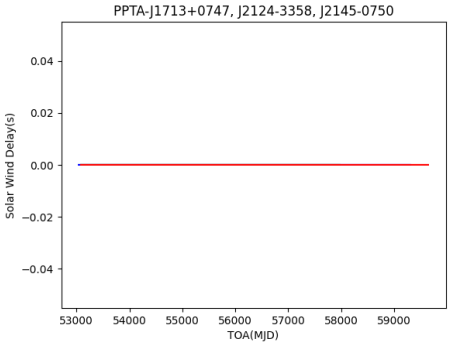


Figure 3: Solar Wind Delay with PINT of PPTA

When calculating the solar wind delay using the SolarWindDispersion() class of pint.models library, the result indicates a solar wind delay of 0.

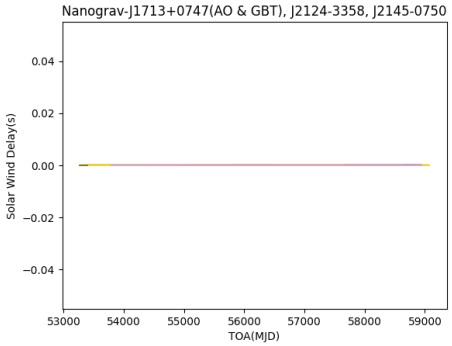


Figure 4: Solar Wind Delay with PINT of NanoGrav

This value is not acceptable. Therefore, we used the NE_SW values from the noise files to construct the following diagrams.

The delay caused by the solar wind is determined by using the formula to calculate the time delay due to radio frequency and the dispersion measure (DM). In this formula, the value of NE_SW of each pulsar replaces the DM. For the Nanograv datasets, since the DMX value absorbs solar wind effects, the solar wind electron density diagrams are less significant. The following diagram illustrates the solar wind delay of individual pulsars from both datasets.

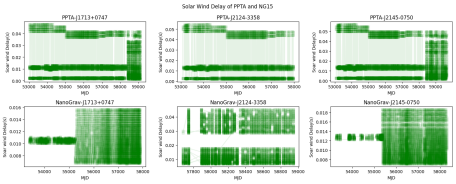

Figure 5: Solar Wind Delay of PPTA and NanoGrav

When the solar wind electron density is fitted to Bayesian modeling for individual pulsars, the results can be observed as in Figure 6 and Figure 7:

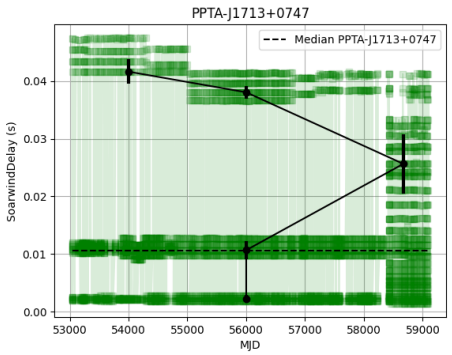


Figure 6: Bayesian Model of Solar Wind Delay of PPTA:J1713+0747

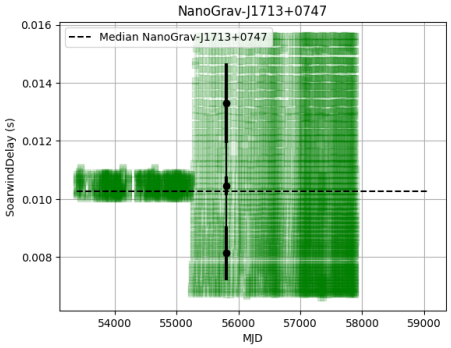


Figure 7: Bayesian Model of Solar Wind Delay of NanoGrav:J1713+0747

Using the same formula for time delay due to DM, the solar wind electron density diagrams are constructed from above solar wind delay data. Those are as in Figure 8. Each figure has a median equal to the NE_SW value of each pulsar.

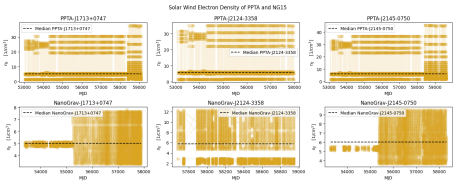

Figure 8: Solar Wind Electron Density of PPTA and NanoGrav

# 4 Discussion

As mentioned, the three diagrams represent the final output of this analysis.

1) Comparison of Sensitivity Curves

From the figure we can draw the following conclusions :

The pulsar designated as J1713+0747 is the most sensitive in both datasets. In the figure, the GBT curve is higher than the other three datasets (PPTA, Nanograv, and Nanograv-AO). The difference in sensitivity curves between GBT and PPTA is approximately 2.911, a significant value. In contrast, the differences among the other curves are within a range of about 1.26, which is negligible.

For the pulsar J2145-0750, the sensitivity curves differ by a factor of approximately 1.235. This difference is appreciable and can be observed in the figure, where the Nanograv curve rises sharply at the minimum frequency.

The sensitivity curves for J2124-3358 present a different scenario. Due to short-timespan data from Nanograv, the difference between the two curves is around a factor of 4.74,

which is substantial compared to the differences observed with the other pulsars.

All the sensitivity curves fit the $f^{-3/2}$ model based on the pulsar spin frequency and are constructed using data from.tim files. Therefore, these curves are based on timing modeling rather than noise modeling. The results may vary if red and white noise is included in the construction of the sensitivity curves.

2)Solar Wind Delay and Solar Wind Electron Density

When using the SolarWindDispersion() class from the PINT library to calculate solar-wind delay, the result is consistently 0 regardless of the pulsar or dataset. This is because the SolarWindDelay() class utilizes the NE_SW values from .par files, which are zero for both the PPTA and NG15-year datasets of each pulsar.

Consequently, the solar wind delay is calculated using NE_SW values from noise files. In the case of the Nanograv dataset, solar wind effects are reflected in the DMX value, necessitating the use of NE_SW values from PPTA noise data files to generate solar wind delay diagrams for both datasets. As noted, the solar wind electron density diagrams are trivial for the Nanograv datasets.

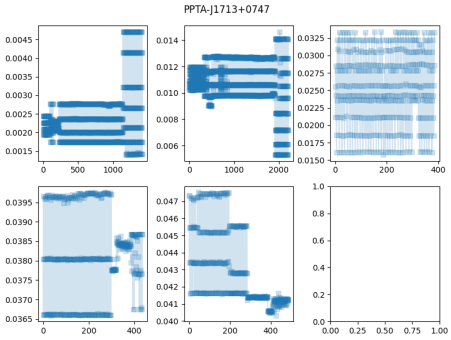


Figure 9: Detailed Solar Wind Delay Diagram of PPTA:J1713+0747

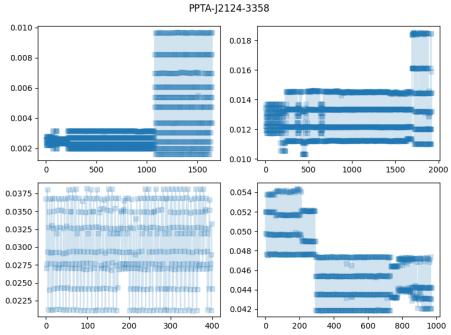


Figure 10: Detailed Solar Wind Delay Diagram of PPTA:J2124-3358

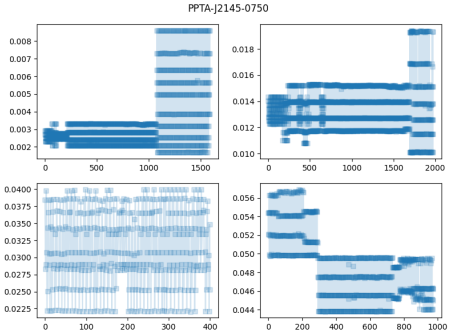


Figure 11: Detailed Solar Wind Delay Diagram of PPTA:J2145-0750

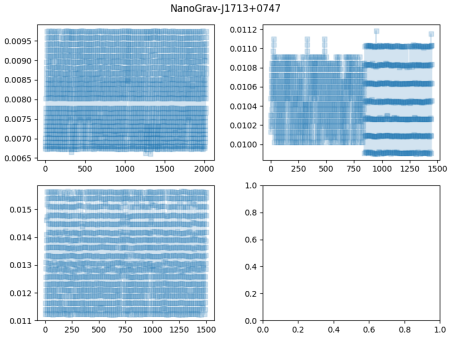


Figure 12: Detailed Solar Wind Delay Diagram of NanoGrav:J1713+0747

The Parkes Telescope operates between 704 and 4032 MHz, with the PPTA data divided into three subbands: 10 cm, 20 cm, and 40 cm. Observations are distributed across these three bands. As a result, the solar wind delay and electron density diagrams exhibit a multilayered distribution, observable in three distinct layers, with the delay or NE values linked to the different bands. The following figures 9,10,11,12 of solar wind delay illustrate more details of each band.

When applying the Bayesian Model to the solar wind delay diagrams, the output is linear, with error bars indicating the uncertainty of the Bayesian model. The subsequent figures 13,14,15,16 display the Bayesian models for solar wind delay across both datasets.

The solar wind electron density is calculated using the same formula, rearranging the terms as necessary. That is represented in Figure 8, specifically for the Nanograv data concerning solar wind electron density diagrams. These figures are insignificant for each pulsar, with the median indicated by a dotted line, which unexpectedly aligns with the NE_SW values for each pulsar. A snippet(Figure 18) from the Collab notebook verifies that the solar wind delay and solar wind electron density calculations are accurate.

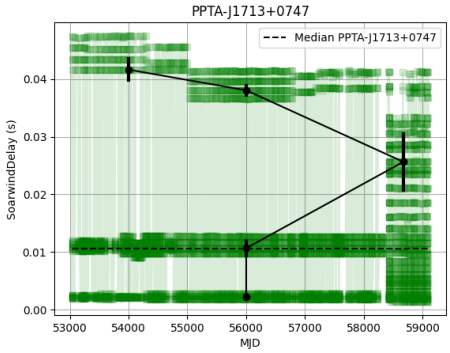


Figure 13: Bayesian Model of Solar Wind Delay Diagram of PPTA:J1713+0747

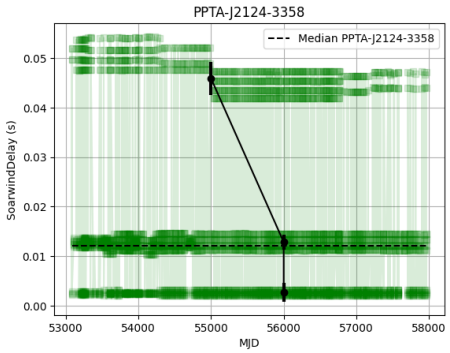


Figure 14: Bayesian Model of Solar Wind Delay Diagram of PPTA:J2124-3358

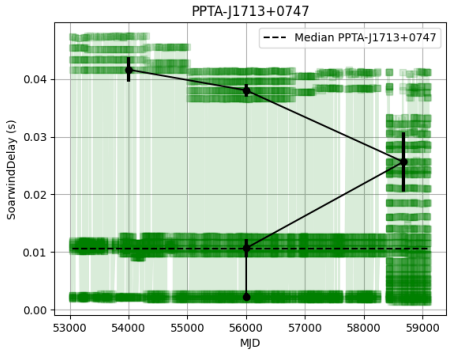


Figure 15: Bayesian Model of Solar Wind Delay Diagram of PPTA:J2145-0750

## Conclusions

The PPTA and Nanograv data sets are valuable to evaluate the sensitivity curves for individual pulsars, except for J2124-3358 and the Nanograv GBT dataset regarding J1713+0747.

The Parkes Telescope operates between 704 and 4032 MHz, with the PPTA data divided into three subbands: 10 cm, 20 cm, and 40 cm. Observations are distributed across these three bands. As a result, the solar wind delay and electron density diagrams exhibit a multilayered

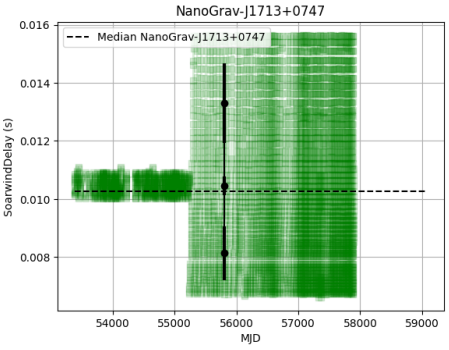


Figure 16: Bayesian Model of Solar Wind Delay Diagram of NanoGrav:J1713+0747

```
mid1 = np.median(np.array(NE_SW_1713_1))
mid2 = np.median(np.array(NE_SW_2124_1))
mid3 = np.median(np.array(NE_SW_2145_1))
mid4 = np.median(np.array(NE_SW_ng_1713))
mid5 = np.median(np.array(NE_SW_ng_2124))
mid6 = np.median(np.array(NE_SW_ng_2145))
mid1, mid2, mid3, mid4, mid5, mid6
```

```
(5.0206514447069015,
 5.7448222498904441,
 6.0118246308458818,
 5.020651444706118,
 5.744822250901903,
 6.011824630845818)
```

```
NE_SW_1713 = 5.0206514446838589999
NE_SW_2124 = 5.744822249890441
NE_SW_2145 = 6.0118246308458179999
```

Figure 17: Collaboratory notebook screenshot for median values of NE_SW

distribution, observable in three distinct layers, with the delay or NE values linked to the different bands. In case of Nanograv, the solar wind is absorbed in the DMX value, thus the delay and solar wind both are evenly distributed throughout, making these diagrams insignificant.

## Acknowledgements

I want to express my gratitude to the team members of NANOGRAV / NANOSTARS at Oregon State University. The author thanks Prof. Jeffery Hazboun for giving this opportunity. As this has been remote work, there was a struggle with everything,from adjusting time zones to learning new concepts.The past team leaders of the team, Phia Morton and Ian Diaz, who helped me a lot during this time. They answered my doubts about the Pulsar Science Collaboratory. Also, I am thankful to Jeremy Baier for his immense help in learning during this project. This project wouldn't have happened if he couldn't have listened to my ideas after reading so many research papers and resolved my queries.

## References


Jeffrey S. Hazboun, Joseph Simon, Dustin R. Madison, Zaven Arzoumanian, H. Thankful Cromartie, Kathryn Crowter, Megan E. DeCesar, Paul B. Demorest, Timothy Dolch, Justin A. Ellis, Robert D. Ferdman, Elizabeth C. Ferrara, Emmanuel Fonseca, Peter A. Gentile, Glenn Jones, Megan L. Jones, Michael T. Lam, Lina Levin, Duncan R. Lorimer, Ryan S. Lynch, Maura A. McLaughlin, Cherry Ng, David J. Nice, Timothy T. Pennucci, Scott M. Ransom, Paul S. Ray, Renée Spiewak, Ingrid H. Stairs, Kevin Stovall, Joseph K. Swiggum, Weiwei Zhu, and The NANOGrav Collaboration. Bayesian solar wind modeling with pulsar timing arrays. *The Astrophysical Journal*, 929(1):39, apr 2022. doi: 10.3847/1538-4357/ac5829. URL https://dx.doi.org/10.3847/1538-4357/ac5829.

Jeffrey S. Hazboun, Joseph D. Romano, and Tristan L. Smith. Realistic sensitivity curves for pulsar timing arrays. *Phys. Rev. D*, 100: 104028, Nov 2019. doi: 10.1103/PhysRevD.100.104028. URL https://link.aps.org/doi/10.1103/PhysRevD.100.104028.

Gabriella Agazie, Md Faisal Alam, Akash Anumarlapudi, Anne M. Archibald, Zaven Arzoumanian, Paul T. Baker, Laura Blecha, Victoria Bonidie, Adam Brazier, Paul R. Brook, Sarah Burke-Spolaor, Bence Bécsy, Christopher Chapman, Maria Charisi, Shami Chatterjee, Tyler Cohen, James M. Cordes, Neil J. Cornish, Fronefield Crawford, H. Thankful Cromartie, Kathryn Crowter, Megan E. DeCesar, Paul B. Demorest, Timothy Dolch, Brendan Drachler, Elizabeth C. Ferrara, William Fiore, Emmanuel Fonseca, Gabriel E. Freedman, Nate Garver-Daniels, Peter A. Gentile, Joseph Glaser, Deborah C. Good, Kayhan Gültekin, Jeffrey S. Hazboun, Ross J. Jennings, Cody Jessup, Aaron D. Johnson, Megan L. Jones, Andrew R. Kaiser, David L. Kaplan, Luke Zoltan Kelley, Matthew Kerr, Joey S. Key, Anastasia Kuske, Nima Laal, Michael T. Lam, William G. Lamb, T. Joseph W. Lazio, Natalia Lewandowska, Ye Lin, Tingting Liu, Duncan R. Lorimer, Jing Luo, Ryan S. Lynch, Chung-Pei Ma, Dustin R. Madison, Kaleb Maraccini, Alexander McEwen, James W. McKee, Maura A. McLaughlin, Natasha McMann, Bradley W. Meyers, Chiara M. F. Mingarelli, Andrea Mitridate, Cherry Ng, David J. Nice, Stella Koch Ocker, Ken D. Olum, Elisa Panciu, Timothy T. Pennucci, Benetge B. P. Perera, Nihan S. Pol, Henri A. Radovan, Scott M. Ransom, Paul S. Ray, Joseph D. Romano, Laura Salo, Shashwat C. Sardesai, Carl Schmiedekamp, Ann Schmiedekamp, Kai Schmitz, Brent J. Shapiro-Albert, Xavier Siemens, Joseph Simon, Magdalena S. Siwek, Ingrid H. Stairs, Daniel R. Stinebring, Kevin Stovall, Abhimanyu Susobhanan, Joseph K. Swiggum, Stephen R. Taylor, Jacob E. Turner, Caner Unal, Michele Vallisneri, Sarah J. Vigeland, Haley M. Wahl, Qiaohong Wang, Caitlin A. Witt, Olivia Young, and The NANOGrav Collaboration. The nanograv 15 yr data set: Observations and timing of 68 millisecond pulsars. *The Astrophysical Journal Letters*, 951(1):L9, jun 2023. doi: 10.3847/2041-8213/acda9a. URL https://dx.doi.org/10.3847/2041-8213/acda9a.

G. Agazie, J. Antoniadis, A. Anumarlapudi, A. M. Archibald, P. Arumugam, S. Arumugam, Z. Arzoumanian, J. Askew, S. Babak, M. Bagchi, M. Bailes, A.-S. Bak Nielsen, P. T. Baker, C. G. Bassa, A. Bathula, B. Bécsy, A. Berthereau, N. D. R. Bhat, L. Blecha, M. Bonetti, E. Bortolas, A. Brazier, P. R. Brook, M. Burgay, S. Burke-Spolaor, R. Burnette, R. N. Caballero, A. Cameron, R. Case, A. Chalumeau, D. J. Champion, S. Chanlaridis, M. Charisi, S. Chatterjee, K. Chatziioannou, B. D. Cheeseboro, S. Chen, Z.-C. Chen, I. Cognard, T. Cohen, W. A. Coles, J. M. Cordes, N. J. Cornish, F. Crawford, H. T. Cromartie, K. Crowter, M. Curyło, C. J. Cutler, S. Dai, S. Dandapat, D. Deb, M. E. DeCesar, D. DeGan, P. B. Demorest, H. Deng, S. Desai, G. Desvignes, L. Dey, N. Dhanda-Batra, V. Di Marco, T. Dolch, B. Drachler, C. Dwivedi, J. A. Ellis, M. Falxa, Y. Feng, R. D. Ferdman, E. C. Ferrara, W. Fiore, E. Fonseca, A. Franchini, G. E. Freedman, J. R. Gair, N. Garver-Daniels, P. A. Gentile, K. A. Gersbach, J. Glaser, D. C. Good, B. Goncharov, A. Gopakumar, E. Graikou, J.-M. Griessmeier, L. Guillemot, K. Gültekin, Y. J. Guo, Y. Gupta, K. Grunthal, J. S. Hazboun, S. Hisano, G. B. Hobbs, S. Hourihane, H. Hu, F. Iraci, K. Islo, D. Izquierdo-Villalba, J. Jang, J. Jawor, G. H. Janssen, R. J. Jennings, A. Jessner, A. D. Johnson, M. L. Jones, B. C. Joshi, A. R. Kaiser, D. L. Kaplan, A. Kapur, F. Kareem, R. Karuppusamy, E. F. Keane, M. J. Keith, L. Z. Kelley, M. Kerr, J. S. Key, D. Kharbanda, T. Kikunaga, T. C. Klein, N. Kolhe, M. Kramer, M. A. Krishnakumar, A. Kulkarni, N. Laal, K. Lackeos, M. T. Lam, W. G. Lamb, B. B. Larsen, T. J. W. Lazio, K. J.

Lee, Y. Levin, N. Lewandowska, T. B. Littenberg, K. Liu, T. Liu, Y. Liu, A. Lommen, D. R. Lorimer, M. E. Lower, J. Luo, R. Luo, R. S. Lynch, A. G. Lyne, C.-P. Ma, Y. Maan, D. R. Madison, R. A. Main, R. N. Manchester, R. Mandow, M. A. Mattson, A. McEwen, J. W. McKee, M. A. McLaughlin, N. McMann, B. W. Meyers, P. M. Meyers, M. B. Mickaliger, M. Miles, C. M. F. Mingarelli, A. Mitridate, P. Natarajan, R. S. Nathan, C. Ng, D. J. Nice, I. C. Niţu, K. Nobleson, S. K. Ocker, K. D. Olum, S. Osłowski, A. K. Paladi, A. Parthasarathy, T. T. Pennucci, B. B. P. Perera, D. Perrodin, A. Petiteau, P. Petrov, N. S. Pol, N. K. Porayko, A. Possenti, T. Prabu, H. Quelquejay Leclere, H. A. Radovan, P. Rana, S. M. Ransom, P. S. Ray, D. J. Reardon, A. F. Rogers, J. D. Romano, C. J. Russell, A. Samajdar, S. A. Sanidas, S. C. Sardesai, A. Schmiedekamp, C. Schmiedekamp, K. Schmitz, L. Schult, A. Sesana, G. Shaifullah, R. M. Shannon, B. J. Shapiro-Albert, X. Siemens, J. Simon, J. Singha, M. S. Siwek, L. Speri, R. Spiewak, A. Srivastava, I. H. Stairs, B. W. Stappers, D. R. Stinebring, K. Stovall, J. P. Sun, M. Surnis, S. C. Susarla, A. Susobhanan, J. K. Swiggum, K. Takahashi, P. Tarafdar, J. Taylor, S. R. Taylor, G. Theureau, E. Thrane, N. Thyagarajan, C. Tiburzi, L. Toomey, J. E. Turner, C. Unal, M. Vallisneri, E. van der Wateren, R. van Haasteren, A. Vecchio, V. Venkatraman Krishnan, J. P. W. Verbiest, S. J. Vigeland, H. M. Wahl, S. Wang, Q. Wang, C. A. Witt, J. Wang, L. Wang, K. E. Wayt, Z. Wu, O. Young, L. Zhang, S. Zhang, X.-J. Zhu, A. Zic, and The International Pulsar Timing Array Collaboration. Comparing recent pulsar timing array results on the nanohertz stochastic gravitational-wave background. *The Astrophysical Journal*, 966(1):105, apr 2024. doi: 10.3847/1538-4357/ad36be. URL https://dx.doi.org/10.3847/1538-4357/ad36be.